PNAS RESEARCH ARTICLE | EVOLUTION

Metabolic reprogramming underlies cavefish muscular endurance despite loss of muscle mass and contractility

Luke Olsen[a,b], Michaella Levy[a], J. Kyle Medley[a], Huzaifa Hassan[a], Brandon Miller[a], Richard Alexander[a], Emma Wilcock[c], Kexi Yi[a], Laurence Florens[a], Kyle Weaver[a], Sean A. McKinney[a], Robert Peuß[d], Jenna Persons[a], Alexander Kenzior[a], Ernesto Maldonado[e], Kym Delventhal[a], Andrew Gluesenkamp[f], Edward Mager[g], David Coughlin[c], and Nicolas Rohner[a,b,1]

Edited by Neil Shubin, The University of Chicago, Chicago, IL; received March 12, 2022; accepted November 15, 2022

Physical inactivity is a scourge to human health, promoting metabolic disease and muscle wasting. Interestingly, multiple ecological niches have relaxed investment into physical activity, providing an evolutionary perspective into the effect of adaptive physical inactivity on tissue homeostasis. One such example, the Mexican cavefish *Astyanax mexicanus*, has lost moderate-to-vigorous activity following cave colonization, reaching basal swim speeds ~3.7-fold slower than their river-dwelling counterpart. This change in behavior is accompanied by a marked shift in body composition, decreasing total muscle mass and increasing fat mass. This shift persisted at the single muscle fiber level via increased lipid and sugar accumulation at the expense of myofibrillar volume. Transcriptomic analysis of laboratory-reared and wild-caught cavefish indicated that this shift is driven by increased expression of *pparγ*—the master regulator of adipogenesis—with a simultaneous decrease in fast myosin heavy chain expression. Ex vivo and in vivo analysis confirmed that these investment strategies come with a functional trade-off, decreasing cavefish muscle fiber shortening velocity, time to maximal force, and ultimately maximal swimming speed. Despite this, cavefish displayed a striking degree of muscular endurance, reaching maximal swim speeds ~3.5-fold faster than their basal swim speeds. Multi-omic analysis suggested metabolic reprogramming, specifically phosphorylation of Pgm1-Threonine 19, as a key component enhancing cavefish glycogen metabolism and sustained muscle contraction. Collectively, we reveal broad skeletal muscle changes following cave colonization, displaying an adaptive skeletal muscle phenotype reminiscent to mammalian disuse and high-fat models while simultaneously maintaining a unique capacity for sustained muscle contraction via enhanced glycogen metabolism.

evolutionary physiology | skeletal muscle metabolism | physical activity

Throughout evolution, movement and feeding have shaped skeletal muscle physiology—whether by enhancing calcium transients to power "super-fast" contraction in the Toadfish swimbladder, accumulating massive swaths of mitochondria to permit large-scale migration in the Atlantic Bluefin Tuna, or restructuring joint anatomy to power explosive snapping in the Pistol Shrimp (1–3). Indeed, extreme environmental conditions necessitate exaggerated skeletal muscle phenotypes, providing powerful insights into the boundaries of skeletal muscle adaptation and performance. While insightful, research studies into these "locomotor extremes" (4) have remained at a single end of the locomotory spectrum. In fact, in contrast to the examples above, many species have drastically decreased physical activity levels, at times remaining completely inactive for months and possibly even years (5–7). Troglobites are prime examples of such extreme changes to locomotion, with multiple cave dwellers remaining either motionless or adapting a glide-and-rest swimming behavior, in stark contrast to their above-ground counterparts (8). While adaptive, these extreme feats of "laziness" beg the question of how skeletal muscle remodels in response to such prolonged changes in activity—periods often spanning millennia—a question present models are unable to address. To this point, we establish the Mexican cavefish as a comparative model to provide an evolutionary perspective into skeletal muscle physiology following dramatic changes in activity levels.

The tetra species *Astyanax mexicanus* is found throughout Mexico and South Texas and is comprised of river-dwelling surface fish and cave-dwelling cavefish. Approximately 160,000 y ago, ancestral surface fish invaded surrounding caves, resulting in multiple independently evolved cave populations (9, 10). Many of these colonized caves are completely devoid of light, resulting in diminished biodiversity and food availability. Consequently, cavefish have adapted a suite of morphological, metabolic, and behavioral traits permitting survival in their nutrient-depleted conditions. For example, cavefish have evolved metabolic strategies such as hyperphagia, enhanced fat storage, insulin resistance, and hyperglycemia (11–13). Additionally, because these cave communities typically have

Significance

The evolutionary consequence of changes to physical activity upon skeletal muscle physiology remains unexplored. Using the Mexican cavefish, we find that loss of moderate-to-vigorous swimming following cave colonization results in broad shifts in skeletal muscle investment—away from muscle mass and instead toward fat and sugar accumulation—ultimately decreasing muscle fiber twitch kinetics. Surprisingly though, cavefish possess marked muscular endurance, reaching maximal swimming speeds rivaling their river-dwelling counterpart. Multi-omic analysis revealed carbohydrate metabolic reprogramming as a contributing component, most notably elevated abundance and phosphorylation of the enzyme phosphoglucomutase-1—a likely consequence of cave-specific hypoxia. These findings emphasize the impact multiple selective pressures have on skeletal muscle physiology, providing insight into the extremes of skeletal muscle plasticity under diverse environmental conditions.

The authors declare no competing interest.

This article is a PNAS Direct Submission.

[1]To whom correspondence may be addressed. Email: nro@stowers.org.

This article contains supporting information online at https://www.pnas.org/lookup/suppl/doi:10.1073/pnas.2204427120/-/DCSupplemental.

Published January 24, 2023.

only a single stygobitic vertebrate species (cavefish), they no longer face predation by other species. As a result, cavefish have dramatically changed their swimming behavior, abandoning energetically expensive burst-like swimming and instead relying on slow, continuous movement (14, 15). Thus, the Mexican cavefish have adapted a suite of metabolic and behavioral traits similar to human metabolic disease—insulin resistance, hyperglycemia, fat accumulation, and diminished moderate-to-vigorous activity—providing unique evolutionary insights into the consequence of such phenotypes on skeletal muscle physiology (16, 17). Importantly, cave and surface populations are conspecific and can be raised under identical, controlled laboratory conditions, permitting comparative studies of heritable physiological consequences to decreased strenuous movement following cave colonization (18). As such, here we leverage the *A. mexicanus* system to address the consequence of, and adaptation to, distinct environmental conditions on skeletal muscle physiology following cave colonization—most notably changes to physical activity—providing unique evolutionary insights into the extremes of skeletal muscle adaptation.

Results and Discussion

Shift in Swimming Speed and Body Composition following Cave Colonization. Cavefish have repeatedly lost aggressive and territorial behavior composed of burst-like swimming and instead rely on slow, continuous movement (14, 15, 19). While previous studies have investigated the average velocities of the surface fish and multiple cavefish populations (15), quantitative analysis of maximal swimming speeds during unperturbed tank swimming—an often-challenging task due to the aggressive behavior of surface fish—has not been performed. To address this, recordings of laboratory-reared surface fish (originating from the Rio Choy) and laboratory-reared cavefish (originating from two independently colonized caves—Pachón cave and Tinaja cave) (Fig. 1*A*) were manually cropped at times containing burst-like swimming (fastest swimming bouts in cavefish), and frame-by-frame distances were analyzed (see *Methods*, Movies S1 *A–C*, and Dataset S1). This experimental design revealed both Pachón and Tinaja cavefish swim markedly slower during their fastest swimming bouts, reaching average burst speeds (acceleration-to-deceleration) ~3.7-fold slower (Fig. 1*B*) and maximal speeds (greatest frame-to-frame distance covered) approximately threefold slower (*SI Appendix,* Fig. S1*A*) than surface fish. These findings are consistent with Paz et al. (20), who found that cavefish have reduced angular velocity during a C-start (escape) response. Providing support that these differences are not a consequence of laboratory conditions, video recordings of wild cavefish (Pachón cave) and wild surface fish (Rio Choy) revealed surface fish incorporate sustained moderate swimming—a form of rheotaxis required to remain stationary against the river current—interspersed by vigorous burst-like swimming (Movie S2*A*). In stark contrast, cavefish displayed an uninterrupted glide-and-rest swimming behavior (Movie S2*B*), confirming that cave colonization resulted in a behavioral phenotype lacking both moderate and vigorous swimming.

Skeletal muscle contraction is a key stimulus influencing muscle physiology (21), with multiple disuse models revealing increased fat accumulation and decreased skeletal muscle mass, fiber size, and force production following physical inactivity (22). Because cavefish have reduced their swimming speed following cave colonization (Fig. 1*B* and *SI Appendix*, Fig. S1*A*), we hypothesized that their skeletal muscle would reflect an "inactive" phenotype and hence shift investment away from muscle mass and instead toward fat accumulation. To this point, baseline *A. mexicanus* body composition was gathered using an echo MRI (echoMRI) system (23). Supporting our hypothesis, both Pachón and Tinaja cavefish have less lean mass (mean lean mass: surface fish = 91.6%; Pachón = 65%; Tinaja = 69.3%. Fig. 1*C*) and more fat mass (mean fat mass: surface fish = 8.3%; Pachón = 34.9%; Tinaja = 30.4%. Fig. 1*D*) than surface fish. These findings were confirmed via histological analysis of full-body cross sections (Fig. 1*E*), revealing a near identical shift away from cavefish muscle mass and instead toward fat accumulation (for quantification see *SI Appendix,* Fig. S1*B* and *C*).

To determine the genetic basis underlying the cavefish body composition, we generated surface/Pachón and surface/Tinaja F1 hybrids and measured fat and lean mass via echoMRI. We found the F1 hybrids possessed a body composition similar to the parental surface fish, indicating that the cavefish phenotype is genetically recessive. Crossing the F1 population, an additional generation to acquire surface/Pachón and surface/Tinaja F2 hybrids revealed a wide distribution in both lean and fat mass (Fig. 1 *C* and *D*), suggesting that the cavefish body composition is a polygenic trait and a promising candidate for future QTL analysis.

Seeking to determine the contributing factor(s) underlying the loss in cavefish muscle mass, we measured muscle fiber cross-sectional area—a predominant component driving muscle atrophy (24). To our surprise, the decrease in cavefish muscle mass occurred independent of a reduction in muscle fiber cross-sectional area. In fact, Pachón cavefish tended to have larger muscle fibers than surface fish, findings confirmed in an independent cohort (Fig. 1 *F* and *G*). To determine whether laboratory conditions—specifically regular feeding and constrained movement—contribute to the observed cavefish muscle fiber size, we collected wild *A. mexicanus* from the Pachón cave (cavefish) and Rio Choy (surface fish) and measured their muscle fiber cross-sectional area. Intriguingly, the opposite phenotype was observed—specifically, wild cavefish had ~38% smaller muscle fibers than wild surface fish (Fig. 1 *F* and *G*). While caution must be taken when interpreting these findings due to muscle fiber heterogeneity along the fish body axis (as seen between experiments 1 and 2—Fig. 1*G*), these data nonetheless indicate that, under laboratory conditions, cavefish maintain a muscle fiber size similar to, if not larger than, laboratory surface fish despite their overall decrease in muscle mass and lack of burst-like swimming.

Surprised by these findings, we sought to explore the investment strategies cavefish incorporate to maintain elevated muscle fiber size under laboratory conditions. In brief, muscle fiber growth takes place through two primary mechanisms: i) sarcoplasmic hypertrophy—the increase in muscle fiber size via increasing the noncontractile sarcoplasmic volume (i.e., fats, sugars, and sarcoplasmic proteins) and ii) myofibrillar hypertrophy—the increase in muscle fiber size via myofibrillar accretion (i.e., sarcomeric proteins actin and myosin) (25). Because cavefish lost burst-like swimming (Fig. 1*B*), coupled with their impressive ability to store body-wide energy reserves (23), we reasoned cavefish employ sarcoplasmic hypertrophy at the expense of myofibrillar hypertrophy. Supporting our hypothesis, cavefish skeletal muscle had approximately fourfold greater triglyceride levels (Fig. 1*H*) and approximately sevenfold greater glycogen levels (Fig. 1*I*) than surface fish. Intriguingly, analysis of a recent lipidomic and metabolomic dataset of *A. mexicanus* skeletal muscle revealed that cavefish preferentially accumulate saturated fatty acids, ceramides, and sphingoid bases, while simultaneously decreasing investment in free amino acids, most notably the mTORC1-activating leucine—a lipid and amino acid profile linked to muscle atrophy and diminished contractility (26, 27) (*SI Appendix,* Fig. S1*D*). Reflecting this, fractionation experiments found that cavefish skeletal muscle has an ~25% and ~17% ($P = 0.1736$) decrease in the contractile protein's myosin and actin, respectively (Fig. 1 *J* and *K*). Transmission electron micrographs

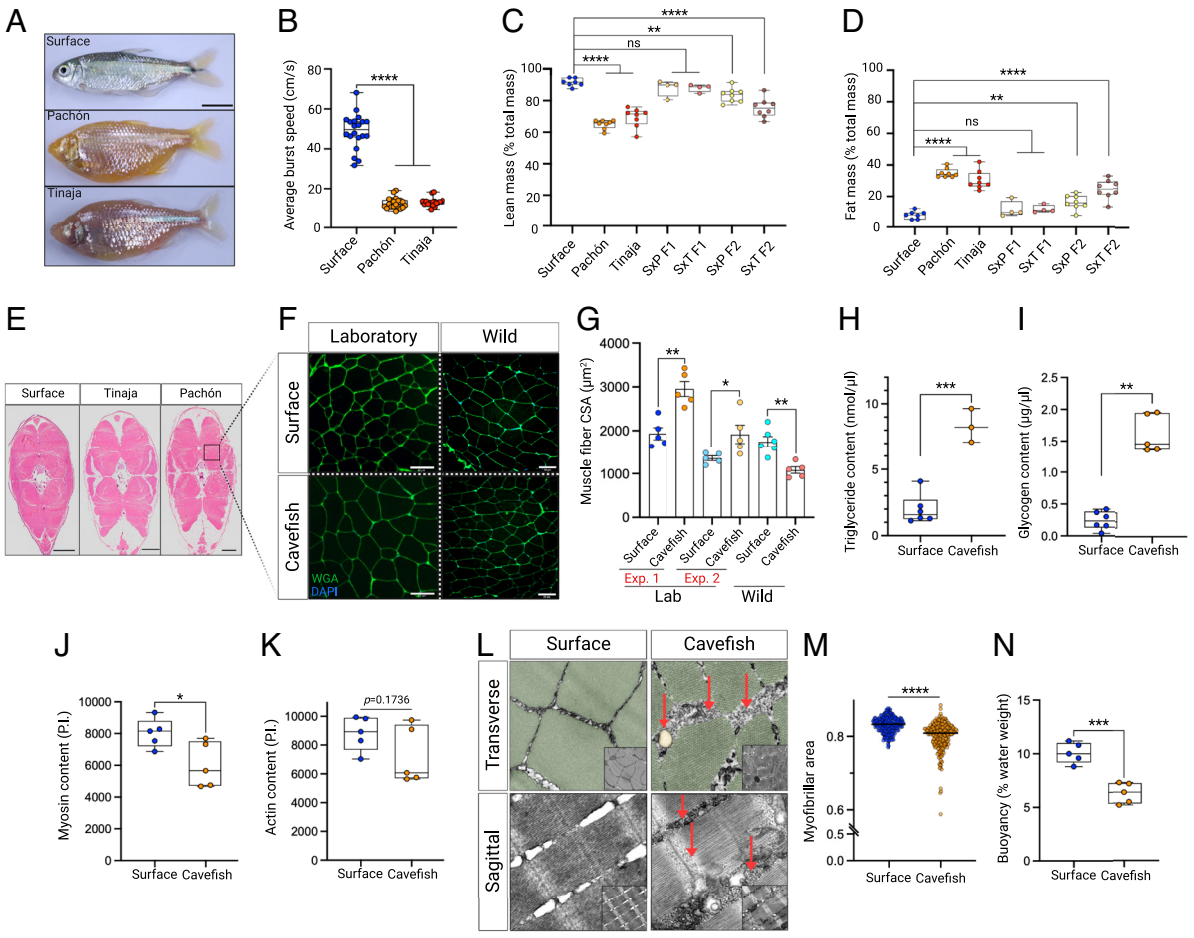

Fig. 1. Shift in cavefish swimming speed and body composition. (*A*) Images of surface fish and two independently evolved cavefish populations: Pachón and Tinaja. (Scale bar, 1 cm.) (*B*) Average burst speed of surface fish, Pachón, and Tinaja cavefish (n = 20, 20, and 18, measurements per population, respectively). Percent (*C*) lean mass and (*D*) fat mass of *A. mexicanus* including F1 and F2 hybrids using an echoMRI (n = 8 for surface, Pachón, and Tinaja; n = 4 for F1 hybrids; n = 8 for F2 hybrids). (*E*) Representative full-body transverse cross sections of *A. mexicanus* used for the echoMRI measurements showing skeletal muscle (pink) and subcutaneous fat (white). (Scale bar, 500 μm.) (*F*) Muscle fiber cross sections from laboratory-reared (*Left*—experiment 1) and wild-caught (*Right*) surface fish and cavefish (Pachón). Muscle fibers are demarcated via wheat germ agglutin (green). (Scale bar, 50 μm.) (*G*) Muscle fiber cross-sectional area (CSA) of laboratory-reared (from experiment 1 and experiment 2) and wild-caught surface fish and cavefish (Pachón). n = 5 for lab Pachón, lab surface, and wild Pachón, n = 6 for wild surface. (*H*) Triglyceride content (nmol/μL) (n = 3 and 6 for Pachón and surface, respectively). (*I*) Glycogen content (μg/μL) (n = 5 and 6 for Pachón and surface, respectively). (*J*) Myosin content in pixel intensity (P.I.) (n = 5 per population). (*K*) Actin content in pixel intensity (P.I.) (n = 5 per population). (*L*) Transverse and sagittal electron micrographs of surface fish and cavefish (Pachón) skeletal muscle (n = 2 per population, scale bar, 200 nm). Green shading highlights the myofibril region and arrows indicate glycogen granules and a lipid droplet. (*M*) Quantification of myofibril area. Each point indicates the relative area of myofibrils within a single EM image. Per sample, ~150 images were quantified. (*N*) Percent water weight of surface fish and cavefish (Pachón). The higher the percent denotes greater weight in water. Following tests for normality (see *Methods*), normally distributed data were analyzed using a one-way ANOVA with Benjamini and Hochberg FDR correction (*C* and *D*) and an unpaired Student's *t* test (*G*, *H*, *J*, *K*, and *N*). Nonnormally distributed data were analyzed using a Kruskal Wallis test with Benjamini and Hochberg FDR correction (*B*) and a Mann–Whitney Wilcox test (*I* and *M*). Data are presented as ±SEM, $*P < 0.05$, $**P < 0.01$, $***P < 0.001$, $****P < 0.0001$, ns = not significant.

supported these findings (Fig. 1*L*), revealing that cavefish muscle fibers have significantly fewer myofibrils with a subsequent increase in sarcoplasmic space relative to surface fish (Fig. 1*M*).

Notably, we observed cavefish muscle fibers have distinct aggregates of glycogen granules both within the intermyofibrillar space (between myofibrils) and intramyofibrillar space (between contractile filaments), with very few granules identified within surface fish (Fig. 1*L* and *SI Appendix*, Fig. S1*E*). These findings are particularly interesting since teleost muscle glycogen stores are presumed to reflect their activity levels—such as the highly active tuna possessing eightfold more glycogen than the sedentary carp (28)—suggesting that cavefish face alternative stimuli resulting in muscle fiber glycogen accumulation (discussed in following sections). We additionally found that cavefish show a distinct increase in infiltrating adipocytes between their slow twitch and fast twitch musculature, which is nearly absent within surface fish (*SI Appendix*, Fig. S1*F*). Intriguingly, we found that the cavefish body composition coincided with an elevated water buoyancy (i.e., weigh less in water) relative to surface fish (Fig. 1*N*). We reason this is a consequence of decreased dense tissue (myofibrils) and increased buoyant tissue (fats). In fact, while the cavefish dry weight was ~20% greater than surface fish (6.05 g vs. 4.84 g, respectively), their water weight was ~22% less than surface fish (0.38 g vs. 0.49 g, respectively). While future work is required to determine the cause or correlative nature of our observations, it nonetheless suggests a thrifty skeletal muscle remodeling strategy incorporated by cavefish to both increase energy reserve capacity while simultaneously improve swimming economy via enhanced static lift—a strategy incorporated by other cave and Antarctic fishes (8, 29)

Change in Cavefish Body Composition Is Reflected at the Level of Gene Expression. Having established a clear shift in cavefish skeletal muscle composition following cave colonization, we next sought to determine whether this change was reflected at the level

of gene expression. To this end, we conducted RNA-sequencing of laboratory-reared surface fish and cavefish skeletal muscle (FDR < 0.01) followed by Gene Ontology (GO) enrichment analysis of the differentially expressed genes (DEGs) (Fig. 2 *A*–*C* and Dataset S2). This revealed several overexpressed pathways related to muscle contractility and structural integrity—specifically "myosin complex" and "actin cytoskeleton" (Fig. 2*C*). Interestingly, most genes within these pathways were downregulated within cavefish, most notably genes encoding fast myosin heavy chain proteins—a class of myosin heavy chains with the capacity for rapid sarcomere cross-bridge cycling (30). In fact, of the DEGs within the myosin complex pathway, ~70% were downregulated within cavefish, decreasing between 18- and 150-fold—all of which were fast myosin heavy chain genes (*SI Appendix,* Fig. S2*A* and Dataset S3). In addition, DEGs contributing to muscle atrophy [*gadd45ga*—(31)] and swimming speed via dopamine suppression [*mblac1*—(32)] were increased and decreased, respectively, within cavefish (*SI Appendix,* Fig. S2 *B* and *C*). Confirming that this transcriptome signature is a cave-specific phenomenon, we sequenced the skeletal muscle from an additional, independently evolved cavefish population (Tinaja cavefish) and found a similar decrease in fast myosin heavy chain expression (Fig. 2*D* and Dataset S4), along with increased and decreased *gadd45ga* and *mblac1* expression, respectively (*SI Appendix,* Fig. S2 *B* and *C*), indicating a conserved decrease in expression of genes necessary for rapid muscle contraction following cave colonization.

To determine whether the above findings are a consequence of domestication, specifically constrained movement due to laboratory housing, we collected additional wild *A. mexicanus* from the Pachón cave and wild surface fish from the San Antonio River and conducted RNA-sequencing of their skeletal muscle. Principal component (PC) analysis revealed a clear discrimination between both environmental conditions (wild/laboratory—PC1) and fish ecotypes (Pachón/surface fish—PC2) (Fig. 2*E*), consistent with previous comparative transcriptome datasets (33). Using a relaxed FDR threshold of <5% to broadly detect changes in gene

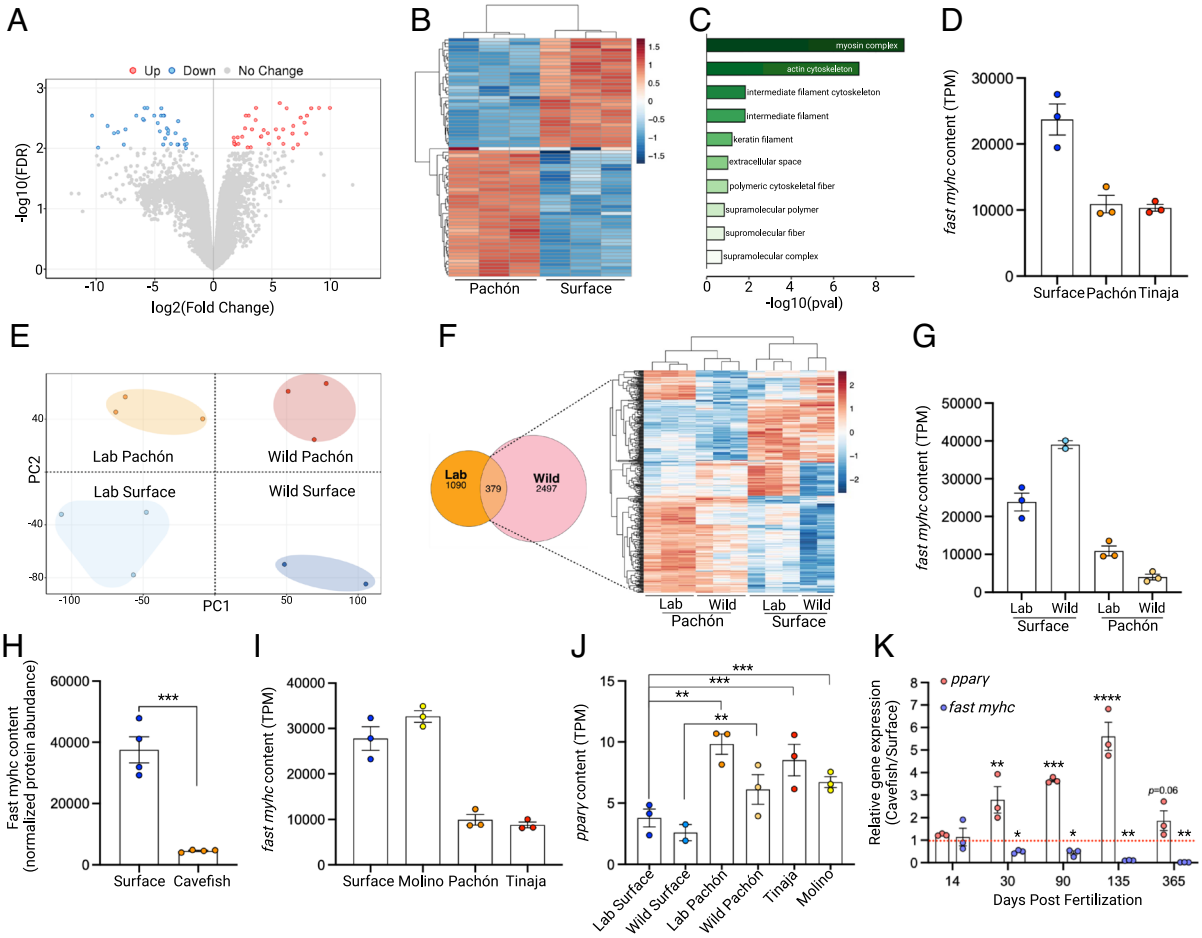

Fig. 2. The cavefish skeletal muscle transcriptome reflects their body composition. (*A*) Volcano plot of the DEGs between laboratory-reared surface fish and cavefish (Pachón) (up- and down-regulated in Pachón fish relative to surface fish). (*B*) Heatmap of the DEGs showing individual replicate data. (*C*) GO enrichment analysis of the DEGs from *A* and *B*. (*D*) Cumulative abundance of shared differentially expressed fast myosin heavy-chain genes in Tinaja and Pachón relative to surface fish (TPM: transcripts per million). (*E*) PC analysis of the laboratory-reared and wild-caught Pachón and surface fish transcriptome. (*F*) Venn diagram of all DEGs between laboratory-reared and wild-caught fish. Specific emphasis is placed on the 379 overlapping genes with their expression shown in the adjacent heatmap. (*G*) Cumulative abundance of the shared differentially expressed fast myosin heavy chain genes between laboratory-reared and wild-caught Pachón and surface fish. (*H*) Cumulative abundance of the differentially expressed fast myosin heavy chain proteins between cavefish (Pachón) and surface fish (n = 4 per population). (*I*) Cumulative abundance of fast myosin heavy chain genes of those identified as significantly different between laboratory-reared Pachón vs laboratory-reared surface fish. These genes (Dataset S6) were then used to determine cumulative fast myosin heavy-chain abundance in Molino and Tinaja. (*J*) *pparγ* expression between all fish populations. (*K*) *pparγ* and fast myosin heavy chain (*fast-myhc*) expression across developmental time points measured via RT-qPCR. Expression is taken relative to surface fish (indicated by the red line). Statistical analysis for RNA-sequencing is described in the "Lab Fish RNA-Sequencing" section in the *SI Appendix, Supplementary Methods*. For *K*, data were analyzed via two-way ANOVA with Benjamini and Hochberg FDR correction. *D*, *G*, and *I* are combined TPM's of multiple fast myosin heavy chain genes and thus additional statistical analysis was not conducted and instead the total TPM abundance is shown. Data are presented as ±SEM, **P* < 0.05, ***P* < 0.01, ****P* < 0.001, *****P* < 0.0001.

expression, we compared the DEGs of the wild samples (2,876 DEGs) against the DEGs of the laboratory samples (1,469 DEGs), revealing 379 overlapping DEGs between populations—the majority differentially expressed in the same direction (Fig. 2*F* and Dataset S5). GO-term analysis of the 379 genes again revealed actin cytoskeleton and myosin complex as the top-ranked differentially regulated pathways (*SI Appendix,* Fig. S2*D* and Dataset S5). Similar to our laboratory transcriptome dataset, 80% of the genes within the myosin complex pathway were downregulated within wild cavefish—decreasing from 2.6- to 85-fold—all of which were fast myosin heavy chain genes (Fig. 2*G*). Validating our RNA-seq data, global proteomic analysis of whole muscle lysate from cavefish and surface fish found an approximately eightfold decrease in fast myosin heavy chain protein abundance in cavefish compared to surface fish (Fig. 2*H*), denoting a conserved reduction at both the transcript and protein level.

The above findings are crucial to account for the impact environmental factors have on skeletal muscle gene expression and confirm that the skeletal muscle phenotypes observed within laboratory cavefish are largely representative of cavefish in the field. However, we questioned whether these phenotypes might reflect phenotypic plasticity and not genetic inheritance. Specifically, might the decreased swimming speed of cavefish in both laboratory and wild conditions be the sole contributor to their reduced "contractile" skeletal muscle phenotype—a possible reflection of the "use it or lose it" phenomenon (34)? To address this, we conducted RNA-sequencing of a phylogenetically younger cavefish population originating from the Molino cave (termed Molino cavefish). Molino cavefish are considered a "new" *A. mexicanus* cavefish lineage—having colonized their cave ~110,000 y ago—and genomically cluster more closely to Rio Choy surface fish than to Pachón or Tinaja cavefish [(10), *SI Appendix* Fig. S3]. Importantly though, Molino cavefish have converged on similar swimming behaviors to Pachón and Tinaja cavefish, lacking territorial and aggressive behavior and thus lacking vigorous swimming (15). With this unique mix of genetic and behavioral traits, we reasoned that if the decrease in fast myosin heavy chain expression is solely a result of phenotypic plasticity (i.e., slow swimming), fast myosin heavy chain expression within Molino cavefish should decrease regardless of their genetic background. Intriguingly, in contrast to the phenotypic plasticity hypothesis, Molino cavefish possessed approximately threefold greater fast myosin heavy chain levels than both Pachón and Tinaja cavefish—levels similar to surface fish (Fig. 2*I*). These findings indicate that the decreased fast myosin heavy-chain expression in Pachón and Tinaja is likely not a result of phenotypic plasticity but instead is driven by genetic inheritance. However, it should be noted that a subset of lowly expressed fast myosin heavy chain isoforms were shifted in a cave-like direction within Molino (i.e., shifted in a similar direction to Pachón and Tinaja), reflecting minimal, but not absent, myosin heavy-chain divergence following Molino cave colonization (Dataset S6).

Cavefish Show Increased Expression of Genes Involved in Skeletal Muscle Lipid Metabolism. In contrast to decreased fast myosin heavy chain expression, cavefish skeletal muscle showed a consistent, and significant, 1.77- to 2.59-fold increase of the master regulator of adipogenesis *pparγ*. This was observed in both wild and laboratory cavefish—including Pachón, Tinaja, and Molino—relative to wild and laboratory surface fish (Fig. 2*J*). In fact, an RT-qPCR time-course analysis found that cavefish gradually increase skeletal muscle *pparγ* expression as early as 30 d post fertilization which continued to adulthood, in contrast to the temporal dynamics of fast myosin heavy chain gene expression which declined early in development and persisted to adulthood (Fig. 2*K*). These findings support our recent discovery of Tinaja, Pachón, and Molino cavefish encoding a truncated variant of period 2—affecting its inhibitory *pparγ*-binding domain—a variant we validated is present in cavefish skeletal muscle (23). Congruently, cavefish muscle had elevated expression of the lipid metabolism genes adiponectin b (*adipoqb*), ceramide synthase 4-b (*cers4b*), adiponutrin (*pnpla3*), and the leptin receptor (*lepr)* (*SI Appendix,* Fig. S2 *E–H*). It should be noted, however, that these additional lipogenic genes only reached statistical significance within the Pachón cavefish and not Tinaja cavefish, suggesting a more extreme "fatty" skeletal muscle phenotype within the Pachón cave population. Collectively, these data support a cavefish skeletal muscle profile indicative of a shift away from skeletal muscle mass/contractility and instead toward fat accumulation, findings strongly reflecting their body composition in Fig. 1.

Functional Analysis of *A. mexicanus* Skeletal Muscle. The skeletal muscle phenotype described above has repeatedly been shown to result in muscle fiber functional decline—most notably diminished muscle fiber contraction—in both rodents and humans (35, 36). While this phenotype is likely beneficial within the starvation-prone cavefish, intramyocellular fat accumulation is poised to result in a functional decline in muscle fiber twitch kinetics. Seeking to address whether a similar physiological consequence occurs within cavefish, we conducted ex vivo muscle bundle contractility experiments (shown in Fig. 3*A*, Movie S3, and described in *SI Appendix*). In brief, live muscle bundles containing ~20 muscle fibers were dissected and tied into a muscle mechanics chamber with a servomotor at one end and a force transducer at the other and platinum electrodes along each side of the chamber. This ex vivo approach is essential to exclude external confounding factors such as differences in neural innervation. In agreement with our hypothesis, cavefish indeed demonstrated a trade-off in muscle contractility, having an ~17% reduction in muscle bundle shortening velocity (Fig. 3*B*), taking ~12% longer to reach maximal force (time from stimulus until maximum isometric force—Fig. 3*C*), and taking ~25% longer to relax following muscle contraction (time from maximum force to 50% relaxation—Fig. 3*D*) relative to surface fish.

Cavefish Maintain the Capacity to Increase Swimming Speeds under Stimulated Conditions. To test if the decreased ex vivo muscle contractility in cavefish results in decreased swimming speed in vivo, we implemented an incremental swim test wherein cavefish and surface fish gradually (5 cm/s every 5 min) increase swimming speeds until volitional fatigue (Fig. 3*E* and Movies S4 *A* and *B*). We found that cavefish reach maximal swimming speeds ~15% slower than surface fish (cavefish: 45.76 cm/s, surface fish: 53.41 cm/s—Fig. 3*F*). Surprisingly though, while slower than surface fish, cavefish showed an impressive ~3.5-fold capacity to increase their swimming speed between their incremental swim test (45.76 cm/s—Fig. 3*F*) and their average burst speed during tank swimming (12.84 cm/s—Fig. 1*B*), whereas surface fish remained largely unchanged between their incremental swim test (53.41 cm/s—Fig. 3*F*) and their average burst speed during tank swimming (48.86 cm/s—Fig. 1*B*). Differences can be seen in *SI Appendix,* Fig. S4*A*. Indeed, conducting the incremental swim test with an additional cavefish population (Tinaja cavefish) revealed a similar ~3.9-fold increase in maximal swimming speed relative to baseline swimming speeds. In fact, Tinaja cavefish reached maximal swim speeds similar to surface fish (Tinaja cavefish: 53.11 cm/s), with no significant difference between populations (Fig. 3*F* and *SI Appendix,* Fig. S4*A* and Movie S4*C*). These data indicate that

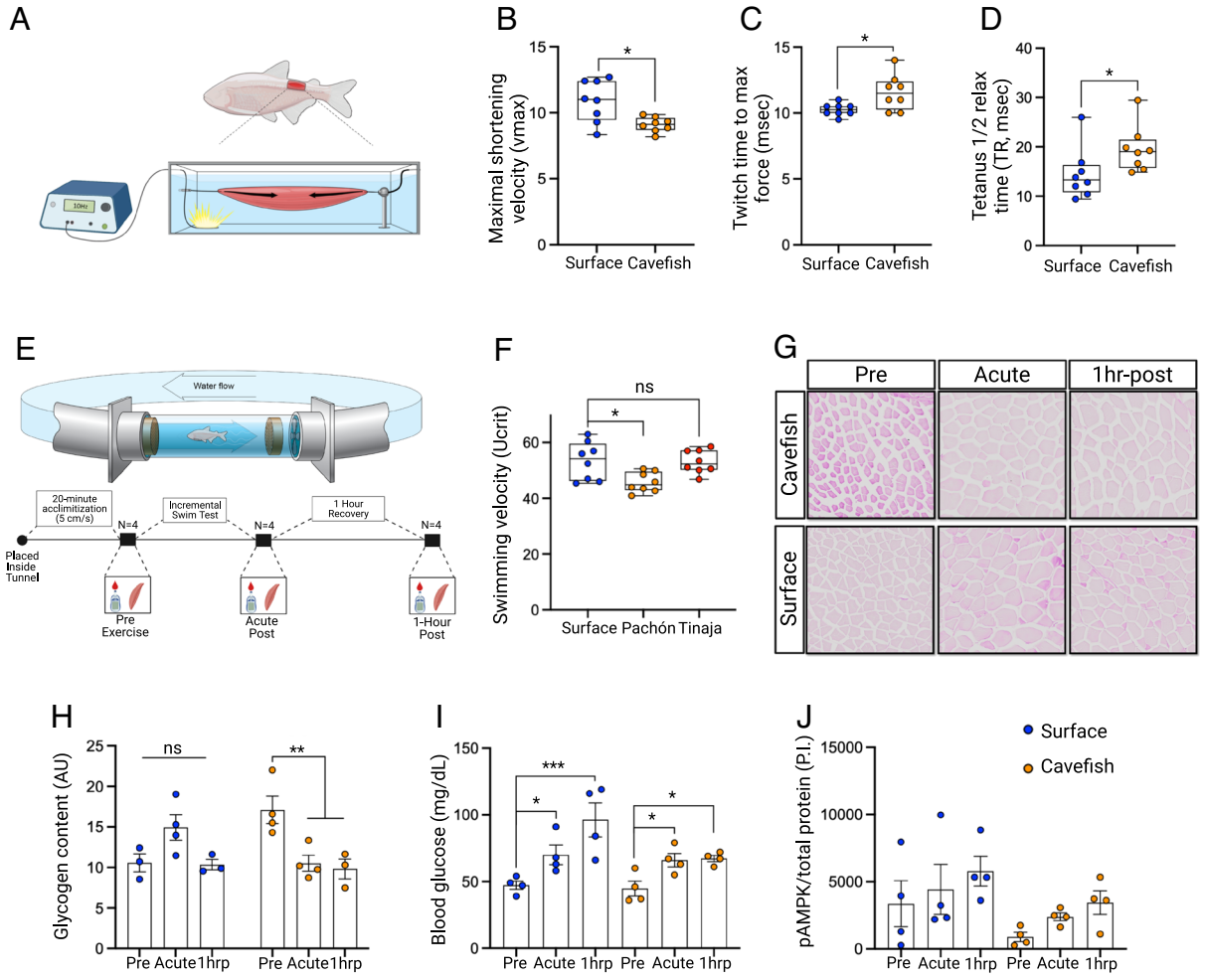

Fig. 3. Cavefish maintain the capacity to increase swim speeds despite reduced muscle contractility. (*A*) Schematic of the muscle mechanics chamber showing skeletal muscle dissection, attachment, and stimulation. Arrows denote muscle shortening. (*B*) Maximal shortening velocity (vmax). (*C*) Twitch time to maximal force (ms). (*D*) Tetanus ½ relax time (TR, ms) (n = 8 per population for each experiment). (*E*) Schematic of the swim tunnel with the experimental timeline of the incremental swim test and tissue/blood collection. (*F*) Maximal swimming speed reached during the incremental swim test (Ucrit in cm/s; *SI Appendix*, Supplementary Methods) for Ucrit equation) in surface fish and cavefish (Pachón and Tinaja) (n = 8 per population). (*G*) Histological images of muscle fiber glycogen via Periodic acid-Schiff stain at the pre, acute-post, and 1-h post time point of surface fish and cavefish (Pachón). (*H*) Quantification of glycogen content shown in *G* (n = 3 to 4 per time point). (*I*) Blood glucose levels of exercised and nonexercised surface fish and cavefish (Pachón) (n = 4 per time point). (*J*) Quantification of phosphorylated AMPK-Thr^{172} in the exercised and nonexercised surface fish and cavefish (Pachón) (n = 4 per time point). Following tests for normality, significance was determined with an unpaired Student's *t* test (*B* and *C*), Mann–Whitney Wilcox test (*D*) one-way ANOVA with Benjamini and Hochberg FDR correction (*F*), and an ordinary, two-way ANOVA with Benjamini and Hochberg FDR correction (*H–J*). Data are presented as ±SEM, $*P < 0.05$, $**P < 0.01$, $***P < 0.001$, ns = not significant.

cavefish have a marked ability to not only increase their swim speed under stimulated conditions but also maintain elevated swim speeds for extended periods of time (each swim test lasted ~40 min), a particularly striking display of muscular endurance for an animal irregularly exposed to such stimuli (discussed in more detail in the *Discussion*).

Cavefish Have Greater Glycogen Utilization during Exercise. We next sought to characterize the molecular mechanisms underpinning cavefish muscular endurance. Because the incremental swim test served as an anaerobic stimulus and since muscular endurance is a function of glycogen levels (37), we reasoned that the elevated glycogen stores within cavefish skeletal muscle (Fig. 1 *I* and *L* and *SI Appendix*, S1*E*) provide the needed metabolic substrate for sustained ATP production and muscle contraction and hence render cavefish fatigue-resistant despite reduced muscle mass and contractility. To address this, we collected skeletal muscle from cavefish and surface fish before, immediately following (acute-post) and 1-h following (1 hrp) the incremental swim test (Fig. 3*E*). This experimental design confirmed that cavefish have greater glycogen levels in the rested state; however, these levels significantly decreased (denoting utilization) both immediately following and 1-h following exercise with no change in surface fish (Fig. 3 *G* and *H*)—these findings are consistent with Salin et al. (38) who found elevated cavefish glycogen utilization following metabolic perturbations relative to surface fish. To confirm the incremental swim test served as a sufficient metabolic stimulus in both fish populations, we analyzed blood glucose levels at all time points and found that both surface fish and cavefish significantly increased blood glucose at the acute and 1 hrp time points (Fig. 3*I*). Additionally, we observed a similar, albeit insignificant, increase in phosphorylated AMPK-Thr^{172}— a common proxy of cellular energetic stress—in both surface fish and cavefish (Fig. 3*J*). As such, these data confirm that the incremental swim test served as a sufficient metabolic stimulus and, importantly, confirmed that cavefish have i) elevated glycogen stores in the rested state and ii) rapidly utilize these stores following the incremental swim test, an indication of cavefish possessing enhanced skeletal muscle glycogen metabolism.

Multi-omic Analyses Suggest Increased Cavefish Glycogen Metabolism. To determine the cellular mechanisms underlying the enhanced cavefish glycogen metabolism, we performed unbiased proteomics via liquid chromatography-tandem mass spectrometry (LC-MS/MS) on the exercised and nonexercised skeletal muscle samples described above (Fig. 4*A* and Dataset S7). Notably, conducting a KEGG pathway analysis of the top 50 ranked proteins identified "glycolysis/gluconeogenesis" as the most differentially regulated pathway with all proteins in this pathway increased in cavefish (Fig. 4*B* and Dataset S8). To confirm and further expand upon our findings, we conducted a targeted proteomic analysis of the same samples and found that half of the proteins within the glycolytic pathway (Aldoa, Eno1, Gapdh, Pfkm, and Pgk1) were significantly increased within cavefish, along with the glycogen handling enzymes phosphoglucomutase 1 (Pgm1), glycogen phosphorylase (Pygm), and the enzyme lactate dehydrogenase (Ldh) (Fig. 4*C* and Dataset S9*A*)—findings reflected by two independent transcriptomic datasets (*SI Appendix,* Fig. S4 *B–I*). Further supporting these findings, analysis of a publicly available metabolomics dataset from *A. mexicanus* skeletal muscle (27) revealed a significant 1.7-fold increase of the glycolytic end product pyruvate within cavefish skeletal muscle relative to surface fish (*SI Appendix,* Fig. S4*J*). Taken together, these datasets confirm a cavefish skeletal muscle profile capable of elevated glycogen metabolism.

Cavefish Skeletal Muscle Has Increased Pgm1 Phosphorylation and Activity. While intriguing, we were hesitant to use static protein and metabolite levels as proxies for dynamic metabolic activity. Phosphorylation is a key regulator of metabolism and has been demonstrated to regulate carbohydrate metabolic dynamics (39), leading us to reason that differential phosphorylation could more accurately reflect enzymatic flux. To this point, a subset of the digested proteins used for proteomics was enriched for phosphorylated peptides via sequential enrichment from metal oxide affinity chromatography (40) followed by LC-MS/MS.

This pipeline identified 430 phosphorylated peptides on 124 proteins in ≥2 biological replicates (Dataset S10). Three-dimensional PC analysis of all phosphorylated peptides revealed a clear separation by population (PC1) and a less dramatic separation by time point (PC2; PC3) (*SI Appendix,* Fig. S4*K*)—findings similarly reflected in human acute exercise omic datasets (41). With a particular interest in the elevated capacity for glycogen storage and utilization within cavefish, we focused on enzymes directly regulating glycogen metabolism. We considered Pgm1 a promising candidate since it i) acts in a bidirectional manner, capable of reversibly synthesizing or degrading glycogen dependent on the energetic stimulus and ii) was identified as one of the most highly phosphorylated proteins at the pre timepoint in cavefish muscle relative to surface fish (Dataset S11). In fact, our phosphoproteomic data revealed that of the four detected Pgm1 phosphorylated sites (Fig. 4*D*), three (Pgm1-Ser^{117}, Pgm1-Thr^{115}, and Pgm1-Thr^{19}) were increased at the pre timepoint 1.7-, 3-, and 5.5-fold, respectively (Fig. 4*E*). Phosphorylation levels on these sites were then uniformly decreased immediately following exercise [similar to recent findings in exercised rodents (42)], followed by a sharp increase at the 1 hrp time point—all of which were greater in the cavefish (Fig. 4 *D* and *E*). These findings indicate that in both basal and recovery states, cavefish have hyperphosphorylation of Pgm1 relative to surface fish, suggesting that phosphorylation of Pgm1 is a crucial node in cavefish glycogen metabolism.

Previous work identified the above phosphorylation sites are essential for Pgm1 activity, with the phospho-serine Pgm1-Ser^{117} required for the interconversion between glucose-1-phosphate to glucose-6-phosphate (or vice-versa), thus serving as a prerequisite for Pgm1 enzymatic activity (43). Notably, missense mutations (threonine-to-alanine) of Pgm1-Thr^{115} and Pgm1-Thr^{19} have been found in humans, resulting in exercise intolerance due to glycogenosis (44, 45). As such, with elevated phosphorylation of all three phosphosites in cavefish skeletal muscle, we reasoned that they would in turn have increased Pgm1 activity. To test this, we measured the Pgm1 activity of biopsied *A. mexicanus* skeletal muscle and found that cavefish have significantly greater Pgm1 activity relative to surface fish (Fig. 4*G*). Importantly, the enhanced cavefish Pgm1 activity was abolished following dephosphorylation via incubation with calf alkaline intestinal phosphatase (CIP) (Fig. 4*F* and *SI Appendix*, S4*L*). In fact, we found cavefish Pgm1 to be more sensitive to dephosphorylation, with its activity reduced below surface fish levels following CIP incubation.

Seeking to directly test the effect Pgm1 phosphorylation has on glycogen metabolism, we utilized CRISPR-Cas9 technology to generate a loss-of-function Pgm1-Thr^{19} mutation, swapping the threonine to the nonphosphorylatable alanine (Pgm1-T^{19}A) within the rat L6 myoblast cell line. Proteomic analysis confirmed the expected amino acid substitution and its sole expression within the Pgm1-T^{19}A cell line (Dataset S13). Supporting the functional role of Pgm1-Thr^{19} on cellular physiology, we found that Pgm1-T^{19}A had ~40% decreased enzymatic activity (Fig. 4*G*), resulting in decreased cellular proliferation relative to Pgm1-WT (Fig. 4*H*). We next used a Seahorse XF Analyzer to measure cellular glycolytic activity via the glycolytic stress test. Intriguingly, supplementing the cellular media with a saturating dose of glucose significantly increased the extracellular acidification rate (ECAR)—a proxy for glycolysis—within Pgm1-T^{19}A relative to Pgm1-WT (Fig. 4 *I* and *J*). Injecting the mitochondrial ATP synthase inhibitor oligomycin further increased glycolysis within Pgm1-T^{19}A relative to Pgm1-WT, reflecting heightened glycolytic capacity within the Pgm1-T^{19}A cells (Fig. 4 *I* and *K*).

Considering Pgm1's ability to bidirectionally regulate glycolysis and glycogen synthesis, the above data suggest that phosphorylation of Pgm1-Thr^{19} preferentially shifts its activity toward glycogen synthesis which, when no longer phosphorylated, shuttles incoming glucose into glycolysis. In agreement, Pgm1-WT synthesized greater levels of glycogen relative to Pgm1-T^{19}A following an insulin and glucose stimulus (Fig. 4*L*). These data agree with the temporal dynamics of Pgm1-Thr^{19} phosphorylation within cavefish (Fig. 4*E*), having increased phosphorylation during energetically favorable time points (pre/1 hrp) and decreased phosphorylation during energetically challenging time points (acute-post). Collectively, the increased Pgm1 phosphorylation in general (Fig. 4*D*), and Pgm1-Thr^{19} phosphorylation in specific (Fig. 4*E*), strongly suggests that cavefish utilize Pgm1 phosphorylation to regulate skeletal muscle glycogen metabolism and may be an important contributor to their muscular endurance.

The above data agree with van der Weele and Jeffery (46) and Medley et al. (27) who found elevated carbohydrate transcripts and metabolites, respectively, within multiple cavefish tissues relative to surface fish. In fact, we recently found primary cavefish liver-derived cells have increased glycolytic capacity relative to surface fish liver-derived cells (47). We propose that this is an adaptation to their hypoxic cave environment. Field studies from our lab have shown that *A. mexicanus* caves have water oxygen saturation levels of 59% compared to 80% in surface fish waters (48). Hypoxia is a strong selective pressure (46, 49, 50), necessitating cavefish to increase reliance on anaerobic metabolism to supply the needed ATP for survival and, more specifically, increase investment in carbohydrate enzyme abundance and phosphorylation to meet their energetic demands. In fact, while two-dimensional and three-dimensional electron micrographs,

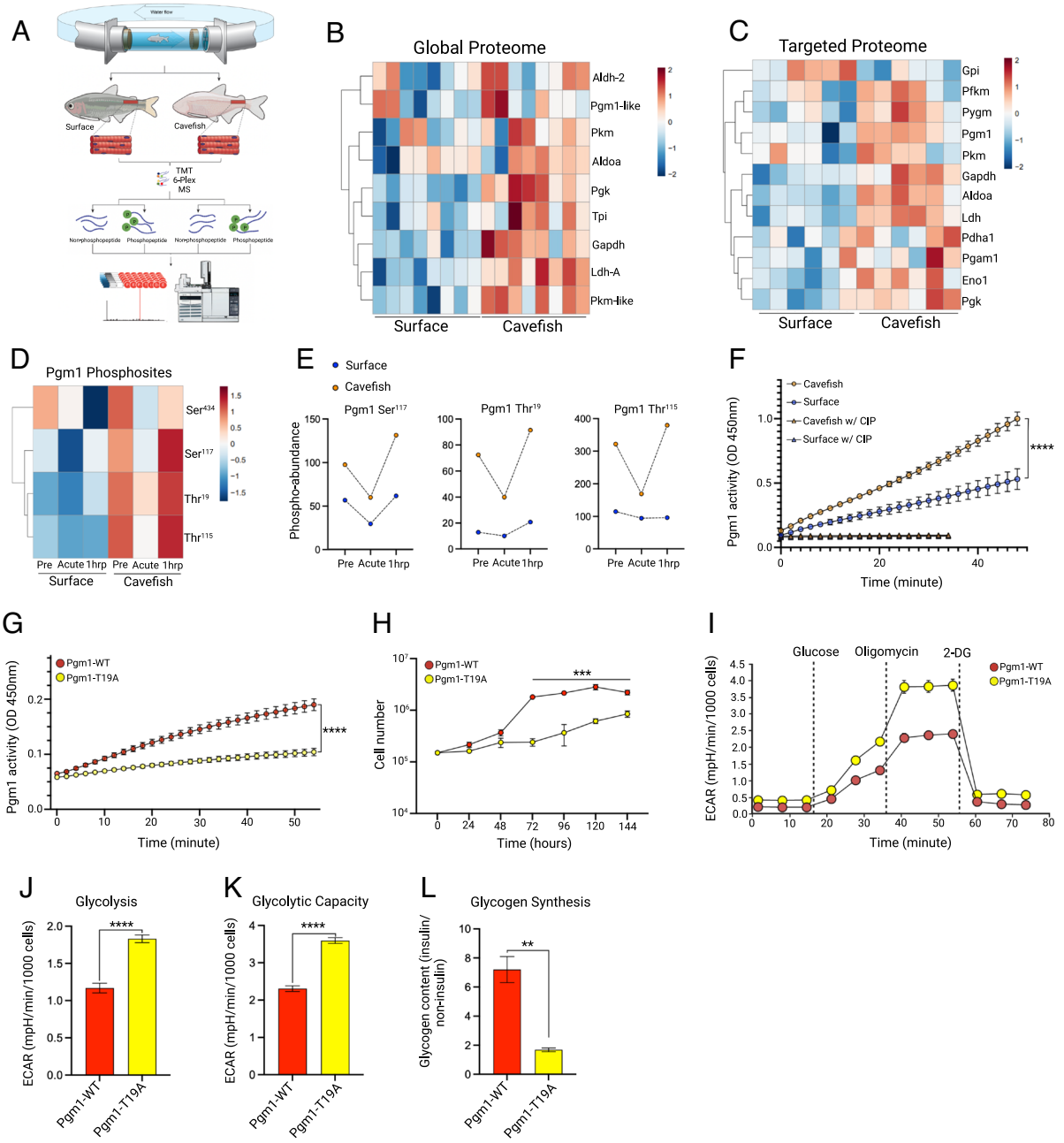

Fig. 4. Multi-omics indicate increased abundance and activity of cavefish carbohydrate enzymes. (*A*) Tissue processing pipeline for both the proteomic and phosphoproteomic analysis for the surface fish and cavefish (Pachón) (n = 4 per time point). (*B*) Heatmap from the global proteomic dataset of the proteins within the glycolysis/gluconeogenesis KEGG pathway (n = 8 per population). (*C*) Heatmap of protein abundance levels from the targeted proteome analysis of proteins regulating carbohydrate metabolism (n = 6 per population). (*D*) Heatmap of the mean peak intensity of Pgm1 phosphorylated sites at the pre, acute, and 1 hrp time points. (*E*) Mean peak intensity of phosphorylation at each time point of surface fish and cavefish (Pachón) for Pgm1-Ser^{117}, Pgm1-Thr^{19}, and Pgm1-Thr^{115}. (*F*) Pgm1 activity assay showing change in fluorescence over time in treated (with CIP) and untreated (without CIP) skeletal muscle samples from surface fish and cavefish (Pachón) (n = 6 per population). (*G*) Pgm1 activity assay of Pgm1-WT and Pgm1-T^{19}A L6 myoblasts (n = 3 biological replicates). (*H*) Cell proliferation assay showing change in cell number spanning 144 h with Pgm1-WT and Pgm1-T^{19}A L6 myoblasts (n = 2 biological replicates). (*I*) ECAR following glucose, oligomycin, and 2-deoxyglucose infusion. (*J*) Difference in glycolysis (maximum rate measurement before oligomycin injection minus last rate measurement before glucose injection). (*K*) Difference in glycolytic capacity (maximum rate measurement after oligomycin injection minus last rate measurement before glucose injection). (*L*) Glycogen synthesis (fold-change in glycogen content following insulin + glucose infusion). Significance was determined using a repeated measures two-way ANOVA (*F* and *G*) and ordinary (nonrepeated) two-way ANOVA (*H*) with Benjamini and Hochberg FDR correction and an unpaired Student's *t* test (*J*, *K*, and *L*). For proteomic and phosphoproteomic data, analysis can be found in the methods. Data are presented as ±SEM, $^{**}P < 0.01$, $^{***}P < 0.001$, $^{****}P < 0.0001$.

along with immunohistochemistry approaches, indicated that cavefish have similar mitochondrial morphology and distribution relative to surface fish (*SI Appendix*, Fig. S5 *A* and *B* and Movie S5), western blot analysis revealed a marked decrease in mitochondrial abundance (*SI Appendix*, Fig. S5*C*). These data further suggest a shift away from the oxygen-dependent metabolism within the skeletal muscle. As such, while future work is required to definitively address the effect differential phosphorylation has on in vivo glycogen metabolism and ATP production, our proteomic and phosphoproteomic data strongly suggest a cavefish skeletal muscle profile well-adapted for carbohydrate metabolism—equipping cavefish with a surprising degree of muscular endurance under stimulated swimming conditions despite the loss of muscle mass and contractility—highlighting the diverse skeletal muscle plasticity following cave colonization.

Discussion

Our results highlight the remarkable breadths of skeletal muscle plasticity within the *A. mexicanus*. Caves pose many challenges to survival—diminished food, decreased oxygen, and complete darkness—resulting in extreme behavioral, morphological, and physiological adaptations. Using surface and cave populations of *A. mexicanus*, we provide convincing evidence that a particularly important site of structural and metabolic reprogramming following cave colonization is the skeletal muscle. Cavefish have made large-scale shifts in their muscle investment, resembling disuse and high-fat conditions commonly seen within mammalian models (17). Indeed, with the loss of predators, water flow, and territorial behavior, cavefish have relaxed investment into skeletal muscle mass and contractility and instead shifted investment toward fat and sugar accumulation. Despite this, cavefish have adapted their metabolism to both increase and maintain elevated swimming speeds under stimulated conditions—findings we hypothesized to result from elevated muscle glycogen levels and utilization during stimulated exercise. Follow-up proteomic and phosphoproteomic analyses of exercised *A. mexicanus* skeletal muscle supported this hypothesis, revealing both protein and phosphorylation levels of key glycogenolytic and glycolytic enzymes increased within cavefish—a phenomenon we reasoned results from their hypoxic cave environment. Indeed, similar adaptations are observed in animals residing in hypoxic environments such as the subterranean African naked mole rat, which relies on fructose-dependent glycolysis under anoxic conditions (51).

Of particular interest, we found hyperphosphorylation of the glycogenolytic/synthetic enzyme Pgm1 and that its phosphorylation resulted in increased Pgm1 activity within cavefish skeletal muscle. Interestingly, the loss-of-function mutation of one of these phosphosites, Pgm1-T^{19}A, within L6 myoblasts shuttled incoming glucose toward glycolysis and decreased insulin-stimulated glycogen synthesis, suggesting that this phosphosite is necessary to shift Pgm1 activity toward synthesizing incoming glucose to glycogen. In fact, human phosphoproteome data found increased Pgm1-Thr^{19} phosphorylation following an insulin infusion—a well-established stimulus of glycogen synthesis (52). Moreover, intact Pgm1 is required for glycogen synthesis under hypoxic conditions (53). We thus reason that the elevated glycogen stores within cavefish skeletal muscle are, at least in part, a result of Pgm1-Thr^{19} phosphorylation and likely serve as a crucial node in cavefish skeletal muscle metabolism providing a surprising degree of muscular endurance despite the loss of muscle mass and contractility. However, it should be noted that in addition to hypoxia, periodic cave flooding and thus elevated water flow cannot be ruled out as a potential stimulus influencing cavefish skeletal muscle metabolism. Occasional flooding within the Pachón and Tinaja cave can, at times, lead to swift water flow exiting the mouth of the cave. As such, adapting the ability to withstand periodic water flow to mitigate being swept away may serve as a crucial survival strategy.

Methods

Additional methods can be found in the *SI Appendix*.

Laboratory Fish Husbandry. *Astyanax* husbandry and care were conducted identical to Xiong et al. (23) and were approved by the Institutional Animal Care and Use Committee (IACUC) of the Stowers Institute for Medical Research on protocol 2021-122. All methods described here are approved on protocol 2021-129. Housing conditions meet federal regulations and are accredited by AAALAC International.

Video Tracking and Tank Burst Swimming. Three fish (either Pachón, Tinaja, or surface) were placed in a 3-L water tank with continuous water circulation for 2 wk prior to recording to acclimate to the surroundings. Fish were then recorded for 2 h beginning at 1,200 and concluding at 1,400 h. Each video was marked at specific times containing the fastest fish movements. For surface fish, this consisted of true bursts–aggressive behavior between two fish. For Pachón and Tinaja fish, the fastest swimming bouts often consisted of accelerations following a turn. Each swim clip began at the beginning of acceleration and concluded at the beginning of deceleration. Subsequent video processing, analysis, and accompanying video legends can be found in *SI Appendix*, Supplementary Methods.

Wild Sample Collection and Tissue Processing. Wild fish collection in Mexico was collected as previously described (33) and conducted under permit No. SGPA/DGVS/03634/19 granted by the Secretaría de Medio Ambiente y Recursos Naturales to Ernesto Maldonado. Samples of wild surface fish were collected from the San Antonio River at San Antonio Zoo, Texas, under Scientific Research Permit SPR-0513-065 granted by Texas Parks and Wildlife Department to Andy Gluesenkamp. For RNA-sequencing, skeletal muscle was dissected immediately posterior to the dorsal fin and submerged in RNAlater until further analysis (1 to 2 wk from initial collection). Immediately upon arrival to the final destination, skeletal muscle was gently blotted to remove RNAlater and placed in 1 mL Trizol (Ambion). Subsequent processing for RNA extraction and sequencing is identical to that described below (*Lab fish RNA sequencing*). For histological analysis, skeletal muscle was dissected from the same region as that used for RNA-seq (separate fish) and immediately submerged in 100% ethanol. Tissue remained in ethanol until further processing (~2 wk). Muscle fiber processing for cross-sectional area measurements was then conducted identical to that described below except images were gathered at 40× (*Lab fish muscle fiber size*).

EchoMRI™ 1100 Analyzer. Here, ~1-y-old fish were used to measure body composition using the EchoMRI™ 1100 Analyzer. In brief, fish were fasted overnight followed by euthanization via ms222 (IACUC, 2021-129). Fish were weighed, measured, and descaled prior to analysis. Female fish had their eggs removed prior to the assay. The echoMRI was calibrated via measurement of a set amount of canola oil. Following calibration, samples were measured with technical replicates with the average as the readout for each sample. Total lean mass and total fat mass were normalized to total body weight and indicated as percent lean mass and percent fat mass.

Histology Processing for EchoMRI™ Samples. Following processing with the EchoMRI™, fish were measured for length/weight and muscle was dissected across the entire trunk–approximately 3 cm from the base of the tail–and placed in 4% paraformaldehyde (PFA) at 4 °C for 5 d. The tissue was subsequently washed in 1× PBS (pH 7.4) for 2 × 15 min at room temperature and then placed in 15% sucrose-1× PBS overnight. The samples were moved to 30% sucrose-1× PBS at 4 °C followed by hematoxylin and eosin staining. Samples were imaged with a VS120 virtual slide microscope (Olympus) and analyzed with ImageJ. To quantify muscle mass, the muscle area was taken relative to the total body area within each section. Care was taken to only use high-quality sections avoiding any tissue damage. Two technical replicates were used for each biological replicate.

Lab Fish Muscle Fiber Size. Skeletal muscle was collected from cavefish and surface fish which were ~1 y in age and similar in size [mean body weight (grams) for experiments 1 and 2: cavefish: 3.183 g, surface fish: 2.481 g]. Muscle tissue was fixed in 4% PFA for 72hrs at 4 °C followed by 2 × 6 min washes in 1× PBS at room temperature and dehydrated by serial incubations in ethanol. Tissue samples were embedded in paraffin and sectioned at a thickness of 10 µm. Sections were deparaffinized, rehydrated in 1× PBS, and blocked in cold 4%BSA/PBS-1%Tween for 15 min. Sections were incubated in 1% wheat germ agglutin rhodamine (RL_1022) in 4%BSA/PBS/1%Tween for 40 min in the dark at room temperature followed by additional 3 × 10 min washes in PBS-1%Tween. Sections were mounted with Vectashield antifade mounting medium with DAPI (Vector laboratories #93952-25). Images were gathered at 10× resolution with a Zeiss Axioplan 2e. The site of muscle fiber selection and analysis is detailed in *SI Appendix*, Supplementary Methods.

Myofibrillar Extraction and Electrophoresis. The myosin and actin fractionation methods were conducted, with slight modifications, as described by Roberts et al. (54). In brief, 20 mg of dorsal muscle tissue was dissected and immediately

submerged in 500 µL of homogenization buffer (98% RIPA lysis extraction buffer (ThermoFisher #89900), 1% Halt protease/phosphatase inhibitor cocktail (Thermo Scientific #78442), 1% EDTA). The tissue was homogenized with triple pure M-Bio grade high-impact zirconium beads in a Beadbug 6 microtube homogenizer bead beater at 4,900 rpm for 60 s followed by gentle agitation at 4 °C for 60 min. The sample was centrifuged at 4 °C at 3,000 × g for 30 min. The supernatant (cytosolic fraction) was removed and frozen at −80 °C. The pellet was resuspended with 500 µL of homogenization buffer, centrifuged for 10 min at 3,000 × g, and the supernatant was removed followed by two additional washes. The remaining myofibrillar pellet was then immediately frozen and placed at −80 °C until further processing. Electrophoresis of the sarcoplasmic and myofibrillar fractions is detailed in *SI Appendix*, Supplementary Methods.

Muscle Triglyceride Content. Skeletal muscle was assayed for triglyceride content following the commercial triglyceride assay kit (#65336–Sigma) on a 200 PRO microplate reader (TECAN). In brief, overnight fasted surface fish and Pachón cavefish were euthanized via ms222 (IACUC, 2021-129), and skeletal muscle immediately posterior to the dorsal fin was dissected. Then, 100 mg of skeletal muscle was washed with cold 1× PBS and homogenized in 1 mL of 5% NP-40/ddH_2O via 20 strokes with a pestle. Samples were gradually heated from 80 °C to 100 °C within a 5-min timespan and then cooled at room temperature. This process was repeated two times followed by centrifugation at 16,900 × g for 2 min. Samples were diluted 10-fold in ddH_2O. The samples were incubated in provided lipase for 20 min at room temperature followed by the addition of the triglyceride reaction mix and incubated at room temperature for 60 min. Samples were then measured at OD 570 nm. Due to extremely high triglyceride levels in all Pachón samples, repeated dilutions were needed to remain within the working range. However, three Pachón cavefish remained out of range (high triglyceride content) and were thus removed from triglyceride quantification. This did not interfere with the final interpretation of triglyceride levels between surface fish and Pachón cavefish.

Muscle Glycogen Content. Skeletal muscle from the same fish used for the triglyceride quantification was used to measure glycogen content following the protocol within the Glycogen Assay Kit (ab65620). In short, 30 mg of skeletal muscle was dissected from the dorsal musculature, ~3 cm from the base of the tail fin, and homogenized on ice via 20 strokes with a pestle. Samples were boiled at 100 °C for 10 min and then centrifuged at 16,900 × g for 10 min at 4 °C. The supernatant was collected followed by colorimetric analysis with a 200 PRO microplate reader (TECAN). Background controls for each sample were included to confirm minimal interference from cellular glucose. Similar to triglyceride quantification, a Pachón cavefish remained out of range following repeated dilutions resulting in this sample being discarded. This did not interfere with the final interpretation of glycogen levels between surface fish and Pachón cavefish.

Fish Buoyancy. Fish buoyancy was conducted as described in Eastman (55). In brief, adult fish were euthanized in ms222 (IACUC, 2021-129) and patted dry. All fish had their swim bladder removed of air and female fish had their eggs removed. Fish were suspended from a hook that was attached to a weighing scale and their dry weight was measured. Fish were then submerged in water with all air removed, and their weight was measured. The weight within the water was taken relative to their dry weight resulting in their percent water weight.

Lab Fish RNA-Sequencing. All fish used were adult, similar in size, and housed at similar tank densities. Fish were fasted overnight and collected at 09:00 the following morning. Fish were euthanized in 500 mg/L of ms222 (IACUC, 2021-129). Skeletal muscle was extracted immediately posterior to the dorsal fin and snap frozen in liquid nitrogen. Then, ~100 mg of frozen tissue was homogenized in 1 mL Trizol (Ambion) with triple pure M-Bio grade high-impact zirconium beads in a Beadbug 6 microtube bead beater. RNA was then extracted using standard phenol/chloroform extraction. The subsequent RNA pellet was cleaned with the RNeasy Mini Kit (Qiagen #74104) with on-column DNAse digestion (Qiagen #79256). A detailed description of library preparation, sequencing, and analysis can be found in *SI Appendix*, Supplementary Methods.

RT-qPCR. Following an overnight fast, skeletal muscle was extracted from *A. mexicanus* and immediately snap frozen. Then, ~100 mg of frozen tissue was homogenized in 1 mL Trizol (Ambion) with triple pure M-Bio grade high-impact zirconium beads in a Beadbug 6 microtube bead beater. RNA was extracted using standard phenol/chloroform extraction. The subsequent RNA pellet was cleaned with the RNeasy Mini Kit (Qiagen #74104) with on-column DNAse digestion (Qiagen #79256). Then, 1 µg of quality RNA was converted to cDNA with the iScript cDNA synthesis kit (Bio-Rad #1708890). qPCR was conducted as described in *SI Appendix*, Supplementary Methods.

Muscle Ex Vivo Kinetics. Muscle mechanics experiments were carried out at Widener University. For muscle mechanics experiments, fish were sacrificed and hypaxial myotomal muscle was dissected from between the pectoral and pelvic girdles. The extracted muscle was maintained in physiological saline (56) at room temperature. Muscle bundles consisted of 2 to 3 myomeres with a typical live muscle length of 4 to 5 mm and live muscle cross-sectional area of ~1 mm^2. Isolated live bundles were tied with silk thread into a muscle mechanics chamber with a servomotor at one end (Aurora Scientific 318B) and a force transducer at the other (Aurora Scientific 404A) followed by muscle bundle kinetic analysis. Further information can be found in *SI Appendix*, Supplementary Methods.

Incremental Swimming Test. The incremental swim test was performed at the University of North Texas (approved by UNT IACUC #19-011) within a Blazka-style 1,500 mL Loligo Systems swim tunnel (#SW10040). Fish in each group were placed in the tunnel for a 20-min acclimatization period with the water flow set at 5 cm/s. This did not cause any strenuous movement or behavior from any of the fish. Fish within the "control" group were immediately removed following the 20-min acclimatization period and euthanized (IACUC, 2021-129). All other fish immediately followed the acclimatization period with the incremental swimming test consisting of ramping the water flow 5 cm/s every 5 min until the fish reached fatigue. Further detail can be found in *SI Appendix*, Supplementary Methods.

Glucose Measurements. Exercised and nonexercised fish were euthanized via ms222 (IACUC, 2021-129) followed by the caudal fin being removed and blood drawn directly to the AlphaTRAK blood glucose monitoring system.

Periodic Acid-Schiff Stain. Exercised and nonexercised fish had their skeletal muscle dissected immediately anterior to that obtained for the phosphoproteomic analysis and placed in 4% PFA at room temperature for 24 h. The samples were washed for 3 × 15 min in 1× PBS followed by serial dehydration in ethanol 1× PBS and placed at 4 °C for 96 h. Tissue was paraffin embedded, sectioned, deparaffinized, and dehydrated to ddH_2O. Slides were placed in 5% periodic acid for 10 min, rinsed in distilled water for 5 min, and placed in Schiff reagent for 15 min at room temperature. The slides were then washed in warm water for 10 min. Sections were mounted in 50% glycerol/1× PBS and imaged on a VS120 virtual slide microscope (Olympus). Analysis was conducted as described in *SI Appendix*, Supplementary Methods.

Protein Quantification via Western Blot. Approximately, 30 mg of frozen skeletal muscle was submerged in an ice-cold RIPA lysis extraction buffer (ThermoFisher #89900) supplemented with 1% Halt protease/phosphatase inhibitor cocktail (Thermo Scientific #78442) and homogenized with triple pure M-Bio grade high impact zirconium beads in a Beadbug 6 microtube homogenizer. Muscle lysate was gently agitated at 4 °C for 2 h and spun down at 16,000 × g for 20 min. The subsequent supernatant was collected and snap frozen in liquid nitrogen. Protein quantification was determined with a Pierce BCA Protein Assay Kit (Thermo #23227). SDS-Page and western blotting for pAMPK (T172) (CST #40H9) and pAb TOM20 (11802-1-AP) can be found in *SI Appendix*, Supplementary Methods.

Tom20 Immunohistochemistry. Fish of comparable size and age were fasted overnight and euthanized in ms222 (IACUC, 2021-129). Skeletal muscle was collected from identical locations (peripheral musculature, ~3 cm from the tail fin). Skeletal muscle was immediately placed in 4% PFA for 96 h at 4 °C. The samples were washed two times in 1× PBS (7.2 pH) followed by incubation in 15% sucrose/1× PBS and 30% sucrose/1× PBS. Tissue was embedded in OCT and frozen in isopentane. The tissue was then sectioned and stained as described in *SI Appendix*, Supplementary Methods.

Phosphoglucomutase Activity Assay and CIP Incubation. Skeletal muscle from overnight fasted fish was extracted posterior to the dorsal fin and immediately frozen in liquid nitrogen. Frozen skeletal muscle was homogenized in the provided buffer with the Phosphoglucomutase activity assay kit (ab155896 abcam) supplemented with protease and phosphatase inhibitors (CIP-treated

samples contained only protease inhibitors). Samples were then gently agitated at 4 °C for 30 min, spun down, and protein measured using the Pierce BCA Protein Assay Kit (Thermo #23227). For CIP incubation, 10 µg of protein from each sample was incubated in 100 µL 1× CIP buffer and 2 µL CIP (5,000 U/mL) (M0525S NEG) for 30 min at 37 °C. Phosphoglucomutase activity of CIP-treated and non-treated samples were then measured according to the manufacturer's instructions (ab155896 abcam) using a 200 PRO microplate reader (TECAN).

Transmission and Scanning Electron Microscopy. For TEM and SEM, surface and cavefish muscle tissues were dissected and fixed with 50 mM sodium cacodylate (pH 7.4) containing 2.5% PFA and 2% glutaraldehyde. The tissue blocks were postfixed with 2% OsO4 for 2 h and 1% uranyl acetate overnight. After dehydration with a graded ethanol series, samples were infiltrated and embedded into Epon resin (EMS). Ultrathin (80 nm) sections were collected on copper grids, stained with 4% uranyl acetate in 75% ethanol and 2% lead citrate and imaged using an FEI transmission electron microscope at 80 kV. For image quantification, see *SI Appendix*, Supplementary Methods. Methods for serial block face scanning electron microscopy can be found in *SI Appendix*, Supplementary Methods.

Global/Phosphorylated Peptide Extraction. Skeletal muscle tissue from each time point was immediately dissected following euthanization via submersion in ms222 (500 mg/L) (IACUC, 2021-129), frozen in liquid nitrogen, and stored at −80 °C until further processing. For tissue homogenization and protein extraction, 30 mg of frozen skeletal muscle was submerged in 1 mL ice-cold lysis buffer containing 100 mM triethylammonium bicarbonate and 10% SDS with 1× protease/phosphatase inhibitor cocktail and homogenized with triple pure M-Bio grade high impact zirconium beads in a Beadbug 6 microtube homogenizer. The lysate was centrifuged at 16,000 × g for 10 min at 4 °C. The supernatant was collected and measured for protein concentration with the Pierce BCA Protein Assay Kit (Thermo #23227). Sample processing for tandem mass tag labeling, phosphopeptide enrichment, mass spectrometry analysis, database searching, and statistical modeling/ranking are described in *SI Appendix*, Supplementary Methods.

Targeted Proteomics. An additional 10% of the remaining global protein samples were used for targeted proteomics. Samples were diluted 1 µL to 25 µL of Buffer A and were transferred to an autosampler vial. The targeted proteomics samples were analyzed with a similar TMT-SPS-MS3 method to the global analysis with the exceptions that the gradient was shortened to 3 h, and an inclusion list was used with 2 to 3 peptides from each of the 22 targeted proteins (Dataset S9*B*). Dyanmic exclusion was not used. Data were analyzed with Proteome Discoverer 2.4 with SEQUEST-HT against the *A. mexicanus* protein database as used in the global analysis. Data searching and analysis are described in *SI Appendix*, Supplementary Methods.

Generation of L6-Pgm1-T19A Cell Line. CRISPR-Cas technology was used for engineering an L6 mutant cell line. Potential guideRNA target sites were designed using CCTOP (57). The target site was selected by evaluating the predicted on-target efficiency score and the off-target potential (58), in addition to the proximity of the double-strand break to the desired mutation site. The selected guideRNA was ordered as an Alt-R CRISPR-Cas9 sgRNA from Integrated DNA Technologies. The CRISPR-Cas9 generation of L6 Pgm1-T19A was then carried out as described within the *SI Appendix*, Supplementary Methods. Validation of the amino acid substitution was conducted via shotgun proteomics and is described in *SI Appendix*, Supplementary Methods.

L6 Myoblast Proliferation Assay. *Rattus norvigicus* L6 myoblast Pgm1-WT and Pgm1-T19A were seeded in a 6-well culture plate at a density of 50,000 cells per well and supplemented with Dulbecco's modified Eagle's medium (DMEM) containing 4.5 g/L glucose and 10% FBS and placed at 37 °C under 5% CO_2. Cells were subsequently counted every 24 h for up to 144 h on a Cellometer stained with trypan blue. Results are the average of two independent experiments.

L6 Glycolytic Stress Test. Glycolysis was measured from *R. norvigicus* L6 myoblasts (both Pgm1-WT and Pgm1-T19A) using the Seahorse XFe96 extracellular flux analyzer (Agilent Technologies). In brief, L6 myoblasts were grown in DMEM supplemented with 10% FBS. On the day before analysis, cells were seeded in the Seahorse XFe96 96-well plate at a density of 15,000 cells per well. The culture medium was changed 1 h before the assay to unbuffered DMEM (pH 7.4). The ECAR was measured sequentially at the basal level, with glucose (10 mM) and in the presence of ATP synthase inhibitor, Oligomycin (1 µM), and glycolysis inhibitor, 2-deoxy-glucose (50 mM). The key parameters measured sequentially are basal ECAR, glycolysis rate, maximum glycolytic capacity, and glycolytic reserve capacity. A single technical replicate from both Pgm1-T19A and Pgm1-WT did not respond to either glucose or oligomycin infusion, reflecting dead/dying cells, and was thus removed from analysis.

L6 Glycogen Synthesis. Glycogen synthesis was measured from the *R. norvigicus* L6 myoblasts (both Pgm1-wildtype and Pgm1-T19A). In brief, cells were serum-starved in low glucose DMEM for 48 h followed by 2-h incubation in high glucose (4.5 g/L) DMEM supplemented with 1 µg/µL human insulin (Sigma #I9278). Cells were washed 2× in cold 1× PBS, detached with a cell scraper in 400 µL ddH2O, and homogenized with a 25-gauge needle. Samples were then boiled for 10 min at 100 °C and then centrifuged at 16,900 × g for 10 min. The supernatant was collected and measured for glycogen content with a glycogen assay kit (AB65620). Glycogen synthesis (fluorescent intensity) was quantified as the ratio between noninsulin stimulated (n = 1) to insulin stimulated (n = 3) for both Pgm1-WT and Pgm1-T19A.

Statistical Analysis. Statistical analysis other than that of proteomics, phosphoproteomics, and RNA-sequencing data was conducted in GraphPad Prism (9.4.0). All datasets, unless otherwise noted, were tested for normality with Anderson–Darling test, D'Agostino and Pearson test, Shapiro–Wilk test, and Kolmogorov–Smirnov test followed by either parametric or nonparametric statistical analysis. Detailed statistical analysis for proteomics, phosphoproteomics, and RNA-sequencing data can be found under their respective sections in the *Methods*. All raw data and statistical analysis can be found in our open access repository detailed below.

Data, Materials, and Software Availability. The mass spectrometry proteomics data have been deposited to the ProteomeXchange Consortium (59, 60) via the PRIDE partner repository with the dataset identifier PXD024165 and may be accessed through the MassIVE partner repository via ftp with username MSV000086857 and password "OlsenMuscle2021." The RNA-seq datasets can be found at the GEO accession number GSE196531. Original data underlying this manuscript may be accessed after publication from the Stowers Original Data Repository at http://www.stowers.org/research/publications/libpb-1679.

ACKNOWLEDGMENTS. We would like to thank the cavefish facility at the Stowers Institute for cavefish husbandry support, specifically Zachary Zakibe, Molly Miller, Elizabeth Fritz, David Jewell, Franchesca Hutton-Lau, Andrew Ingalls, Diana Baumann, and Adam Petrie. We would like to thank Sylvie Rétaux and Mathilda Mommersteeg for providing wild *A. mexicanus* videos. We thank Mark Miller for assistance with illustrations. Surface/Pachón and surface/Tinaja F1 hybrids were kindly provided by Brian Martineau and Dr. Clifford Tabin. We thank all core support provided by the Stowers Institute; specifically, Seth Malloy, Dai Tsuchiya, and Nancy Thomas of Histology; Cindy Maddera and Christopher Wood of Microscopy; Rhonda Egidy and Amanda Lawlor of Sequencing and Discovery Genomics; Melainia McClain and Fengli Guo of Electron Microscopy; Jailyn Marshall, MaryEllen Kirkman, and Jacob Yonke of Genome Engineering; William Redwine of Custom Protein Resources; and Charles Banks of Proteomics. We thank Subir Roy Chowdhury of KUMC for assistance with the Seahorse XF Analyzer. We would like to especially thank all members of the Rohner Lab for the critical review of our manuscript along with Dr. Gustavo Blanco, Dr. Matt Morris, Dr. Chad Slawson, and Dr. Kausik Si for their critical comments throughout the planning and experimental process. N.R. is supported by institutional funding, NIH Grant 1DP2OD028806-01, NIH Grant R01 GM127872, NSF IOS-1933428, and NSF EDGE award 1923372.

Author affiliations: [a]Stowers Institute for Medical Research, Kansas City, MO 64110; [b]Department of Cell Biology and Physiology, University of Kansas Medical Center, Kansas City, KS 66160; [c]Department of Biology, Widener University, Chester, PA 19013; [d]Institute for Evolution and Biodiversity, University of Münster, Münster 48149, Germany; [e]EvoDevo Research Group, Unidad Académica de Sistemas Arrecifales, Instituto de Ciencias del Mar y Limnología, Universidad Nacional Autónoma de México, Puerto Morelos, Quintana Roo 77580, Mexico; [f]Center for Conservation and Research, San Antonio Zoo, San Antonio, TX 78212; and [g]Department of Biological Sciences, Advanced Environmental Research Institute, University of North Texas, Denton, TX 76203

Author contributions: L.O., M.L., B.M., K.Y., L.F., K.W., K.D., and N.R. designed research; L.O., M.L., B.M., E.W., K.Y., R.P., J.P., A.K., E.M., A.G., E.M., and D.C. performed research; L.O., M.L., J.K.M., H.H., B.M., R.A., E.W., L.F., K.W., S.A.M., R.P., and D.C. analyzed data; and L.O. and N.R. wrote the paper.

1. L. C. Rome, D. A. Syme, S. Hollingworth, S. L. Lindstedt, S. M. Baylor, The whistle and the rattle: The design of sound producing muscles. *Proc. Natl. Acad. Sci. U.S.A.* **93**, 8095–8100 (1996).
2. P. A. Dumesic *et al.*, An evolutionarily conserved uORF regulates PGC1alpha and oxidative metabolism in mice, flies, and bluefin tuna. *Cell Metab.* **30**, 190–200.e196 (2019).
3. T. Kaji, A. Anker, C. S. Wirkner, A. R. Palmer, Parallel saltational evolution of ultrafast movements in snapping shrimp claws. *Curr. Biol.* **28**, 106–113.e104 (2018).
4. M. H. Dickinson *et al.*, How animals move: An integrative view. *Science* **288**, 100–106 (2000).
5. O. Fröbert, A. M. Frøbert, J. Kindberg, J. M. Arnemo, M. T. Overgaard, The brown bear as a translational model for sedentary lifestyle-related diseases. *J. Intern. Med.* **287**, 263–270 (2020).
6. G. Balázs, B. Lewarne, G. Herczeg, Extreme site fidelity of the olm (Proteus anguinus) revealed by a long-term capture–mark–recapture study. *J. Zool.* **311**, 99–105 (2020).
7. D. Hendrickson, J. Krejca, J. Martínez, Mexican blindcats genus Prietella (Siluriformes: Ictaluridae): An overview of recent explorations. *Environ. Biol. Fishes* **62**, 315–337 (2001).
8. K. Hüppop, *How Do Cave Animals Cope with Food Scarcity in Caves?* (Elsevier Press, Amsterdam, 2001).
9. J. B. Gross, The complex origin of Astyanax cavefish. *BMC Evol. Biol.* **12**, 105 (2012).
10. A. Herman *et al.*, The role of gene flow in rapid and repeated evolution of cave-related traits in Mexican tetra, Astyanax mexicanus. *Mol. Ecol.* **27**, 4397–4416 (2018).
11. S. Xiong, J. Krishnan, R. Peuß, N. Rohner, Early adipogenesis contributes to excess fat accumulation in cave populations of Astyanax mexicanus. *Dev. Biol.* **441**, 297–304 (2018).
12. M. R. Riddle *et al.*, Insulin resistance in cavefish as an adaptation to a nutrient-limited environment. *Nature* **555**, 647–651 (2018).
13. A. C. Aspiras, N. Rohner, B. Martineau, R. L. Borowsky, C. J. Tabin, Melanocortin 4 receptor mutations contribute to the adaptation of cavefish to nutrient-poor conditions. *Proc. Natl. Acad. Sci. U.S.A.* **112**, 9668–9673 (2015).
14. Y. Elipot, H. Hinaux, J. Callebert, S. Rétaux, Evolutionary shift from fighting to foraging in blind cavefish through changes in the serotonin network. *Curr. Biol.* **23**, 1–10 (2013).
15. B. M. Carlson, I. B. Klingler, B. J. Meyer, J. B. Gross, Genetic analysis reveals candidate genes for activity QTL in the blind Mexican tetra, Astyanax mexicanus. *PeerJ* **6**, e5189 (2018).
16. N. Rohner, Cavefish as an evolutionary mutant model system for human disease. *Dev. Biol.* **441**, 355–357 (2018).
17. F. W. Booth, C. K. Roberts, J. P. Thyfault, G. N. Ruegsegger, R. G. Toedebusch, Role of inactivity in chronic diseases: Evolutionary insight and pathophysiological mechanisms. *Physiol. Rev.* **97**, 1351–1402 (2017).
18. J. Krishnan *et al.*, Genome-wide analysis of cis-regulatory changes underlying metabolic adaptation of cavefish. *Nat. Genet.* **54**, 684–693 (2022).
19. D. Moran, R. Softley, E. J. Warrant, Eyeless Mexican cavefish save energy by eliminating the circadian rhythm in metabolism. *PLoS One* **9**, e107877 (2014).
20. A. Paz, B. McDole, J. E. Kowalko, E. R. Duboue, A. C. Keene, Evolution of the acoustic startle response of Mexican cavefish. *J. Exp. Zool. B Mol. Dev. Evol.* **334**, 474–485 (2020).
21. M. V. Franchi, N. D. Reeves, M. V. Narici, Skeletal muscle remodeling in response to eccentric vs. concentric loading: Morphological, molecular, and metabolic adaptations. *Front. Physiol.* **8**, 447 (2017).
22. S. S. Rudrappa *et al.*, Human skeletal muscle disuse atrophy: Effects on muscle protein synthesis, breakdown, and insulin resistance–A qualitative review. *Front. Physiol.* **7**, 361 (2016).
23. S. Xiong *et al.*, Enhanced lipogenesis through Pparγ helps cavefish adapt to food scarcity. *Curr. Biol.* **32**, 2272–2280.e2276 (2022).
24. S. C. Bodine, Disuse-induced muscle wasting. *Int. J. Biochem. Cell Biol.* **45**, 2200–2208 (2013).
25. M. D. Roberts, C. T. Haun, C. G. Vann, S. C. Osburn, K. C. Young, Sarcoplasmic hypertrophy in skeletal muscle: A scientific, "unicorn" or resistance training adaptation? *Front. Physiol.* **11**, 816 (2020).
26. D. A. Rivas *et al.*, Sphingosine-1-phosphate analog FTY720 reverses obesity but not age-induced anabolic resistance to muscle contraction. *Am. J. Physiol. Cell Physiol.* **317**, C502–C512 (2019).
27. J. K. Medley *et al.*, The metabolome of Mexican cavefish shows a convergent signature highlighting sugar, antioxidant, and ageing-related metabolites. *Elife* **11**, e74539 (2022).
28. A. M. Sänger, A. M. W. Stoiber, Muscle fiber diversity and plasticity. *Fish Physiol.* **18**, 187–250 (2001).
29. A. L. Devries, J. T. Eastman, Lipid sacs as a buoyancy adaptation in an Antarctic fish. *Nature* **271**, 352–353 (1978).
30. S. Schiaffino, C. Reggiani, Fiber types in mammalian skeletal muscles. *Physiol. Rev.* **91**, 1447–1531 (2011).
31. C. C. Fontes-Oliveira *et al.*, A differential pattern of gene expression in skeletal muscle of tumor-bearing rats reveals dysregulation of excitation–contraction coupling together with additional muscle alterations. *Muscle Nerve* **49**, 233–248 (2014).
32. J. A. Hardaway *et al.*, Glial expression of the Caenorhabditis elegans gene swip-10 supports glutamate dependent control of extra synaptic dopamine signaling. *J. Neurosci.* **35**, 9409–9423 (2015).
33. J. Krishnan *et al.*, Comparative transcriptome analysis of wild and lab populations of Astyanax mexicanus uncovers differential effects of environment and morphotype on gene expression. *J. Exp. Zool. B Mol. Dev. Evol.* **334**, 530–539 (2020).
34. K. M. Wisdom, S. L. Delp, E. Kuhl, Use it or lose it: Multiscale skeletal muscle adaptation to mechanical stimuli. *Biomech. Model Mechanobiol.* **14**, 195–215 (2015).
35. N. K. Biltz *et al.*, Infiltration of intramuscular adipose tissue impairs skeletal muscle contraction. *J. Physiol.* **598**, 2669–2683 (2020).
36. S. J. Choi *et al.*, Intramyocellular lipid and impaired myofiber contraction in normal weight and obese older adults. *J. Gerontol. A Biol. Sci. Med. Sci.* **71**, 557–564 (2016).
37. L. Hermansen, E. Hultman, B. Saltin, Muscle glycogen during prolonged severe exercise. *Acta Physiol. Scand.* **71**, 129–139 (1967).
38. K. Salin, Y. Voituron, J. Mourin, F. Hervant, Cave colonization without fasting capacities: An example with the fish Astyanax fasciatus mexicanus. *Comp. Biochem. Physiol. A Mol. Integr. Physiol.* **156**, 451–457 (2010).
39. L. Chen *et al.*, Effects of protein phosphorylation on glycolysis through the regulation of enzyme activity in ovine muscle. *Food Chem.* **293**, 537–544 (2019).
40. S. I. S. Jae Choi, Ryan Bomgarden, John C. Rogers, *Sequential Enrichment from Metal Oxide Affinity Chromatography (SMOAC), a Phosphoproteomics Strategy for the Separation of Multiply Phosphorylated from Mono-Phosphorylated Peptides* (ThermoFisher Scientific, 2017).
41. K. Contrepois *et al.*, Molecular choreography of acute exercise. *Cell* **181**, 1112–1130.e1116 (2020).
42. G. Maier *et al.*, Transcriptomic, proteomic and phosphoproteomic underpinnings of daily exercise performance and zeitgeber activity of training in mouse muscle. *J. Physiol.* **600**, 769–796 (2021), 10.1113/jp281535.
43. Y. Lee, K. M. Stiers, B. N. Kain, L. J. Beamer, Compromised catalysis and potential folding defects in in vitro studies of missense mutants associated with hereditary phosphoglucomutase 1 deficiency. *J. Biol. Chem.* **289**, 32010–32019 (2014).
44. L. C. Tegtmeyer *et al.*, Multiple phenotypes in phosphoglucomutase 1 deficiency. *N. Engl. J. Med.* **370**, 533–542 (2014).
45. T. Stojkovic *et al.*, Muscle glycogenosis due to phosphoglucomutase 1 deficiency. *N. Engl. J. Med.* **361**, 425–427 (2009).
46. C. M. van der Weele, W. R. Jeffery, Cavefish cope with environmental hypoxia by developing more erythrocytes and overexpression of hypoxia inducible genes. *Elife* **11**, e69109 (2022).
47. J. Krishnan *et al.*, Liver-derived cell lines from cavefish Astyanax mexicanus as an in vitro model for studying metabolic adaptation. *Sci. Rep.* **12**, 10115 (2022).
48. N. Rohner *et al.*, Cryptic variation in morphological evolution: HSP90 as a capacitor for loss of eyes in cavefish. *Science* **342**, 1372–1375 (2013).
49. T. Boggs, J. Gross, Reduced oxygen as an environmental pressure in the evolution of the blind Mexican cavefish. *Diversity* **13**, 26 (2021).
50. T. E. Boggs, J. S. Friedman, J. B. Gross, Alterations to cavefish red blood cells provide evidence of adaptation to reduced subterranean oxygen. *Sci. Rep.* **12**, 3735 (2022).
51. T. J. Park *et al.*, Fructose-driven glycolysis supports anoxia resistance in the naked mole-rat. *Science* **356**, 307–311 (2017).
52. E. J. Needham *et al.*, Personalized phosphoproteomics identifies functional signaling. *Nat. Biotechnol.* **40**, 576–584 (2022).
53. E. Bae, H. E. Kim, E. Koh, K. S. Kim, Phosphoglucomutase1 is necessary for sustained cell growth under repetitive glucose depletion. *FEBS Lett.* **588**, 3074–3080 (2014).
54. M. D. Roberts *et al.*, An optimized procedure for isolation of rodent and human skeletal muscle sarcoplasmic and myofibrillar proteins. *J. Biol. Methods* **7**, e127 (2020).
55. J. T. Eastman, The buoyancy-based biotope axis of the evolutionary radiation of Antarctic cryonotothenioid fishes. *Polar Biol.* **43**, 1217–1231 (2020).
56. F. Seebacher, S. R. Pollard, R. S. James, How well do muscle biomechanics predict whole-animal locomotor performance? The role of Ca2+ handling. *J. Exp. Biol.* **215**, 1847–1853 (2012).
57. M. Stemmer, T. Thumberger, M. Del Sol Keyer, J. Wittbrodt, J. L. Mateo, CCTop: An intuitive, flexible and reliable CRISPR/Cas9 target prediction tool. *PLoS One* **10**, e0124633 (2015).
58. M. Labuhn *et al.*, Refined sgRNA efficacy prediction improves large- and small-scale CRISPR-Cas9 applications. *Nucleic Acids Res.* **46**, 1375–1385 (2018).
59. Y. Perez-Riverol *et al.*, The PRIDE database and related tools and resources in 2019: Improving support for quantification data. *Nucleic Acids Res.* **47**, D442–D450 (2019).
60. E. W. Deutsch *et al.*, The ProteomeXchange consortium in 2020: Enabling "big data" approaches in proteomics. *Nucleic Acids Res.* **48**, D1145–D1152 (2020).